의학박사 학위논문

Collateral Ventilation Quantification Using Xenon-enhanced Dynamic Dual Energy CT

-Detection on Its Difference between Canine and Swine Models of Bronchial Occlusion-

제논 조영증강 동적 이중에너지 CT를 이용한 측부 환기량 정량화

-기관지폐색개와 돼지모델에서의 차이분석-

2014 년 2 월

서울대학교 대학원

의학과 영상의학 전공

박 은 아

제논 조영증강 동적 이중에너지 CT를 이용한 측부 환기량 정량화

-기관지폐색개와 돼지모델에서의 차이분석-

지도교수 구 진 모

이 논문을 의학석사 학위논문으로 제출함

2014 년 1 월

서울대학교 대학원

의학과 영상의학 전공

박 은 아

박은아의 의학박사 학위논문을 인준함

2014 년 1 월

위 원 장 ..... (인)

부위원장 ..... (인)

위 원 ..... (인)

위 원 ..... (인)

위 원 ..... (인)

Collateral Ventilation Quantification Using Xenon-enhanced Dynamic Dual Energy CT

-Detection on Its Difference between Canine and Swine Models of Bronchial Occlusion-

by
Eun-Ah Park

A thesis submitted to the Department of Radiology in partial fulfillment of the requirements for the Degree of Doctor of Philosophy in Medicine (Radiology) at Seoul National University College of Medicine

January 2014

Approved by Thesis Committee:

Professor Chul-Gyu Yoo Chairman
Professor Jin Mo Goo Vice chairman
Professor Jin Wook Chung
Professor Young Tae Kim
Professor Joon Beom Seo

ABSTRACT

Purpose: This study was conducted to evaluate whether the difference in the degree of collateral ventilation between canine and swine models of bronchial obstruction can be detected using xenon-enhanced, dynamic dual energy technique of dual source CT. Through this study, we wanted to evaluate the feasibility of xenon-enhanced, dynamic dual energy technique of dual source CT for the quantification of collateral ventilation.

Methods: Eight adult Mongrel dogs (25~30 kg) and six pigs (25~30kg) were studied under general anesthesia. With fluoroscopic guidance, the posterior segmental bronchus of the caudal lobe was occluded with 11.5 mm standard occlusion balloon catheter. Dynamic dual energy scanning (51 eff. mAs/213 eff. mAs at 140 kV/80 kV) was performed with dual source CT (Somatom Definition, Siemens) at a 12-second interval for 2 minute washin period and 24-second interval for 3 minute washout period while animals were mechanically ventilated via an endotracheal tube (60% xenon). CT images and xenon maps were generated using dedicated software. Ventilation parameters of magnitude (A value), maximal slope,

velocity (K value), and time-to-peak enhancement (TTP) were calculated from dynamic xenon map using exponential function of Kety model.

Results: Pigs showed significant lower maximal enhancement in the occluded than in the patent parenchyma (8.3 ± 1.1 HU vs. 41.3 ± 5.9 HU, p =0.027) but dogs did not show any difference (44.4 ± 8.1 HU vs. 47.2 ± 6.0 HU, p =0.123). Bigger between-parenchyma difference in A value was observed in pigs than in dogs (absolute difference, −33.0 ± 5.0 HU vs. −2.8 ± 7.1 HU, p =0.001; normalized percentage difference, −79.8 ± 1.8% vs. −5.4 ± 16.4%, p =0.0007). Mean values of maximal slopes in both periods significantly decreased in the occluded parenchyma only in pigs (maximal $slope_{washin}$, 4.7 ± 1.9 vs. 6.3 ± 2.8 in dogs, p =0.068; maximal $slope_{washout}$, −10.6 ± 2.8 vs. −8.6 ± 2.8 in dogs, p =0.092; maximal $slope_{washin}$, 1.0 ± 0.2 vs. 5.1 ± 1.5 in pigs, p =0.027; maximal $slope_{washout}$, −1.6 ± 1.4 vs. −10.2 ± 1.7 in pigs, p =0.028). Between-parenchyma absolute and normalized percentage differences in maximal slopes were greater in pigs than in dogs but statistical difference reached only in the washin period (all, p <0.05). K values of both periods were not different in dogs (p =0.892). One the other

hand, in pigs, significant difference was found only in washin period (0.0029 ± 0.0006 sec^{-1} for occluded vs. 0.0039 ± 0.0003 sec^{-1} for patent, p =0.027). While TTP was not significantly different between the occluded and patent parenchyma in dogs (p =0.892), TTP was markedly delayed in the occluded parenchyma in pigs (absolute difference, 212 ± 53.5 s vs. 140 ± 9.8 s, p =0.027; normalized percentage difference, 51.1 ± 34.4% vs. 6.8 ± 33.5%, p =0.013).

Conclusions: Xenon-enhanced, dynamic dual energy technique of dual source CT allows quantifying collateral ventilation and detecting its difference between canine and swine models of bronchial obstruction.

Keywords: Chronic obstructive pulmonary disease, Emphysema, Collateral ventilation, Xenon, Dual energy CT

Student number: 2007-30957

CONTENTS

LIST OF TABLES

LIST OF FIGURES

LIST OF ABBREVIATIONS

COPD, chronic obstructive pulmonary disease

EBV, endobronchial valve

NETT, National Emphysema Treatment Trial

PBV, Perfusion Blood Volume

ROI, regions of interest

TTP, time to peak

INTRODUCTION

The phenomenon of collateral ventilation is defined as the ventilation of gas exchanging airspaces via pathways other than the regular branching airways (1,2). Although the pores of Kohn were first described in the 19th century (3), the significance of collateral ventilation was not described until 1930, when Van Allen noticed no collapse distal to the obstructed bronchus in dogs (4). This significance was largely overlooked by physiologists and physicians alike, apart from several studies reported in the 1960s and 1970s (5-8). However, with the emergence of new bronchoscopic techniques for the treatment of emphysema, collateral ventilation has garnered much renewed interest (2).

Chronic obstructive pulmonary disease (COPD), which is characterized by irreversible and progressive airway obstruction resulting from the destruction of lung parenchyma and inflammatory changes of the large and small airways (9), is one of the leading causes of morbidity and mortality worldwide and is, at present, the fourth most common cause of death among adults (10). Although the diagnosis of COPD is made solely based on pulmonary function test, significant

heterogeneity of clinical presentation and disease progression exists (11,12). Currently, there is evidence to define COPD phenotypes with clinical, prognostic and therapeutic repercussions: "overlap" or mixed COPD-asthma, excerbator, and emphysema-hyperinflation (12).

Emphysema-hyperinflation phenotype is a progressive debilitating disease characterized by irreversible destruction of alveolar tissue. This causes reduced elastic recoil, progressive hyperinflation and gas trapping (13). Patients experience chronic dyspnea, fatigue, reduced exercise tolerance and poor quality of life (14). Patients with severe emphysema remain significantly disabled despite attempts at treatment through pharmacological therapy (15), long-term oxygen therapy and (16) pulmonary rehabilitation (17). These therapies are not able to either remove or reverse the hyperinflation induced by the alveolar destruction, and therefore offer limited benefit.

Lung volume reduction surgery involves the resection of areas of diseased lung to reduce hyperinflation and improve breathing mechanics. The National Emphysema Treatment Trial (NETT)(15) demonstrated that, in patients with emphysema in the upper lobes and low exercise capacity, a mortality was

significantly reduced after lung reduction surgery. However, despite the most careful patient selection, I a three-month postoperative mortality rate and a nonfatal complication rate have been reported to be 5-10% and 60%, respectively (14).

Bronchoscopic lung volume reduction therapy using various materials has been taken to minimize these surgical risks: endobronchial valve (18-20), coil (21), thermal vapor ablation (22) and a polymer sealant (23-25). Endobronchial valves (EBVs) are designed to prevent air from entering into distal lung while allowing air and secretions to escape the lobe. As a result, atelectasis of the treated lobe develops, and the lung volume decreased, resulting in clinical improvement (26). A large prospective, multicenter trial called the Endobronchial Valve for Emphysema Palliation Trial (VENT)(27) was performed to assess the effectiveness of EBV, and has shown no device-related death up to 12 months after treatment. They have shown a wide range of improvement after EBV treatment and attributed it to the degree of collateral ventilation. For this reason, collateral ventilation has garnered much renewed importance in the selection of the patients who might benefit from bronchoscopic lung volume reduction.

Recent studies have shown that xenon ventilation CT using dual energy technique of dual source CT overcomes the variability of lung attenuation caused by different lung volumes between scans(28-35) and is capable of assessing functional regional ventilation by enabling the differentiation of xenon from lung tissue with use of the material decomposition theory (36-39). Dual energy xenon ventilation CT is expected to be able to quantify collateral ventilation by analyzing time-xenon density curve of occluded lung parenchyma after bronchial occlusion. It could be used as a clinical marker for predicting response to EBV treatment.

Development of collateral ventilation varies according to the species, depending on the degree of lobulation of the lung (40,41). In the dog lung, there are no interlobular fibrous septa, whereas in the pig or cow interlobular septa are more extensive and complete than in man and the horse (5,41). Therefore, the present study was designed to evaluate whether the difference in the degree of collateral ventilation between canine and swine models of bronchial obstruction can be detected using xenon-enhanced, dynamic dual energy technique of dual source CT.

MATERIALS AND METHODS

Phantom Study

This phantom study was to determine (a) whether xenon map generated using three decomposition theory from 80 kV and 140 kV images obtained by dual energy CT technique shows attenuation linearity according to xenon concentration, and (b) whether baseline tissue density affects attenuation on xenon map. To validate the first thesis, we prepared four rubber bags and different concentration of xenon was delivered: 0%, 20%, 60% and 90%. To validate the second thesis, we designed two kinds of rubber bags: one contained artificial cotton mimicking lung parenchyma and the other was empty. Xenon of 30% concentration was delivered to both bags.

Dynamic dual energy scanning was performed with dual source CT (Somatom Definition; Siemens Medical Solutions, Forchheim, Germany). Parameters were as follows: a 512x512 pixel matrix, 14x1.2 mm collimation, 51 effective mAs at 140 kV and 213 effective mAs at 80 kV, pitch of 0.45, and gantry rotation time of 0.33 second rotation time. Images were reconstructed with 1.5 mm thickness, in 1.2 mm increments, and soft tissue reconstruction (D30f kernel). Three sets of

images were obtained: an 80 kV image, a 140 kV image, and a mixed image. The images were automatically generated in the CT scanner. From a combination of the 140 kV and the 80 kV image, the mixed image was automatically generated by using the weighting ratio of 3:7 for the ratio of the 140 kV image to the 80 kV image on the CT console. This mixed image is close to an approximately 120 kV image when that weighting ratio is used and can be used for the conventional CT image. By using image data of 80 kV and 140 kV, xenon maps were obtained using commercially available software of the lung Perfusion Blood Volume (PBV) application class of Syngo Dual Energy (Siemens Medical Solutions, Forchheim, Germany), which was based on the material decomposition theory (36). Material parameters were adjusted for xenon extraction as follows: −990 HU for air at 80 kV; −1000 HU for air at 140 kV; 70 HU for soft tissue at 80 kV; 54 HU for soft tissue at 140 kV; 1.95 for relative contrast material enhancement; and 10 for range. Mean densities were measured at each data set.

Animal Study

Animal Preparation

This experiment was approved by our Institutional Animal Care and Use Committee (IACUC No. 10-0012, Study Number 12-2010-001-4; IACUC No. 09-0289, Study Number 12-2010-002-5). Eight adult mongrel dogs (weight range, 30-35 kg) and six adult pigs (weight range, 30-35 kg) were examined during administration of a general anesthetic. Anesthesia was induced with a subcutaneous injection of a mixture of 15 mg/kg Zolazepam (Zoletil ®; Yuhan Corp., Seoul, Korea), 5-10 mg/kg Xylazine hydrochloride (Rompun; Bayer Korea, Seoul, Korea), and 0.02-0.04 mg/kg Atropine Sulfate (Atropine; DAHIHAN pharm, Co., LTD, Seoul, Korea). Then an endotracheal tube with a 7.0-7.5 mm inside diameter was placed.

Bronchial Occlusion

The protocol of bronchial occlusion modeling in a canine was described in detail elsewhere (38). The methods of bronchial occlusion in both canine and swine models was not different. With fluoroscopic guidance, the posterior segmental bronchus of the caudal lobe was occluded with occlusion balloon (Boston-Scientific, Standard occlusion balloon catheter, 11.5 mm) . The balloon catheter was introduced through side hole of connector (Elbow Connector, Swivel; Winnomed Company Ltd,

Taoyuan, Taiwan) interposed between the endotracheal tube and breathing circuit of mechanical ventilator. The catheter tip was manipulated selectively into the posterior segmental bronchus by using a guidewire. Then, the balloon was inflated with 1 mL of a mixture of saline and intravenous contrast material. Davis catheter was placed in the stomach in order to prevent gastric distention before bronchial occlusion. After the location of the occlusion site was checked by using the radiopaque balloon (Figure 1), the catheter was fixed and the balloon was deflated. The animal was moved to the CT room in a prone position to prevent dependent atelectasis in the caudal lobe. After arrival of the animal in the CT room, CT scan was performed to check the location of balloon catheter tip and size of target bronchus. After the balloon was inflated again, CT scan was repeated in order to make sure of complete occlusion of bronchus. The diameter of inflated balloon was 1.5 times bigger than that of bronchus. In general, 1 mL of the mixture of saline and contrast material was used to inflate the balloon 1.5 times bigger than size of bronchus. Before xenon-enhanced CT examination, Davis catheter placed in the stomach was removed to avoid an artifact.

Xenon-enhanced Dynamic Dual-Energy CT Protocol

Dynamic dual energy scanning was performed with dual source CT (Somatom Definition; Siemens Medical Solutions) at a 12-second interval for 2-minute washin period and 24-second interval for 3-minute washout period (Figure 2) (38). A 12 cm thick section around the obstructed site was chosen for baseline unenhanced and dynamic xenon-enhanced CT. Parameters were same as that of the phantom study.

During the washin period, a mixture of 60% xenon and 40% O_2 was inhaled via mechanical ventilator (Servo ventilator 900 C; Simens Elema, Solna, Sweden). The mechanical ventilator was set at 10 cycles per minute at a tidal volume of 10 mL/kg. The inspiration-expiration ratio was set as 1:3. During the wash-out period, replacement O_2 was provided to keep the tidal volume constant after xenon halt.

Lastly, CT scan was performed 1 hour after balloon inflation to check whether the collapse of the occluded segment occurred.

Image Postprocessing

Images were reconstructed with 1.5 mm thickness, in 1.2 mm increments, and soft tissue reconstruction (D30f kernel). Four

sets of images were obtained: an 80 kV image, a 140 kV image, a mixed image and a xenon map. The detailed method was described in the phantom study.

Image Analysis

For quantitative analysis of xenon maps, a board-certificate chest radiologist (P.E.A) selected images obtained at the same anatomic level among dynamic xenon maps. She placed the regions of interest (ROIs) with the same size and same location at selected dynamic xenon maps using a tool of copy and paste of ROI on a PACS workstation (Radmax; Marotech, Seoul, Korea) with 2048 x 1536 pixel 20.8 inch monochrome liquid crystal display monitors (ME315L; Totoku Electric, Tokyo, Japan). ROIs were located in the parenchyma with patent airways and with occluded airways. From the time-attenuation curve of those ROIs, ventilation parameters were calculated by another observer (P.S.J) using in-house software that was based on data analysis software (Matlab; MathWorks Inc, Natick, MA, USA). After subtraction of the baseline attenuation from the mean attenuation of each region of each time point, we fitted each regional washin and washout time-attenuation curve to a single compartment exponential model (Kety model) using

a nonlinear least-squares curve-fitting procedure (32,42). Washin period for calculation was defined until when the peak attenuation reached. In occluded lung parenchyma of pigs, each washin curve was analyzed from the starting point of time attenuation curve to peak attenuation. Parameters of magnitude of ventilation (A value), maximal slopes, and velocity of ventilation (K value) of ROIs were calculated.

Kinetics of Xenon ventilation according to the Kety model is briefly introduced. If a constant concentration of xenon gas is inhaled, alveolar filling and clearance can be exponentially characterized. The concentration of xenon in tissue during inhalation (washin) at a given time t can be expressed as follows:

$$C_t = A(1 - e^{Kt})$$

where Ct is the concentration of inspired gas at time t, and A (in Hounsfield units) is the amount of enhancement of Xenon gas present in the lungs at time infinity and is related to the volume. K is the rate constant (reciprocal of the time constant) that relates alveolar ventilation to alveolar volume ($\dot{V}/V$) (min^{-1}), called specific ventilation. $K = 1/T_{mean}$ = alveolar ventilation/alveolar volume ($\dot{V}/V$) (min^{-1}), where T_{mean} is the

mean transit time. When this CT technique is used, the monitored volume v remains constant and the ventilation rate constant K is directly proportional to the fractional ventilation ($\dot{v}/v$) (32).

Based on Kety model, washin and washout curves can be fitted as an equation below (35).

$$C(t) = \begin{cases} C_0, & t < t_1 \\ A(1 - e^{-Kt}), & t_0 < t < t_1 \\ A * e^{-Kt}, & t > t_1 \end{cases}$$

Above equations show fitting functions based on Kety model. t_1 is a time of arriving at peak point on time attenuation curve.

In addition, time to peak (TTP) was defined as time point when maximal xenon enhancement reached.

Statistical Analysis

The Wilcoxon matched-pairs signed rank test was used to compare ventilation parameters between patent and occluded parenchyma in both animals. In terms of the between-parenchyma differences in ventilation parameters, two kinds of difference values were calculated: (a) absolute difference representing subtraction values of occluded lung from those of patent lung and (b) normalized percentage difference indicating

values of absolute difference divided by those of patent lung and multiplied by 100. The Mann–Whitney U–test was used to compare between–parenchyma differences in ventilation parameters between both animals. All statistical analyses were performed with statistical packages (SPSS 19.0; IBM Corporation, Armonk, NY, USA). Differences were considered significant when the p value was less than 0.05.

RESULTS

Phantom Study

Table 1 summarized CT attenuation according to xenon concentration at each image. We found linear relationship between CT attenuations and xenon concentration (Figure 3).

Figure 4 well demonstrates that the baseline tissue density did not affect CT attenuation on xenon map. CT attenuations of artificial cotton measured in a mixed image were approximately 15 HU higher than the air in the bag containing artificial cotton or the empty bag: −945.4 HU for artificial cotton, −962.8 HU for the air in the bag containing artificial cotton, and −957.5 HU for the air in the empty bag. However, CT attenuations on xenon maps consistently showed similar values about 40 HU in both bags, irrespective of baseline densities of mixed images.

Animal Study

Washin and washout values in both patent and occluded segments based on Kety model could be successfully calculated in all eight dogs (Figure 5). On the other hand, in pigs, whereas washin values of patent and occluded segments could be

calculated in all six pigs, washout values of occluded segment could not be obtained in two pigs because of continuous increase in CT attenuation even during the washout period (Figure 6). Whereas collapse of occluded lung segment did not occur in all eight dogs, complete collapse developed in six pigs 1 hour after balloon occlusion.

Table 2 demonstrates results of ventilation parameters between patent and occluded lung parenchyma in both animals with bronchial occlusion. In a dog model of bronchial occlusion, peak enhancement and maximal slopes during both washin and washout periods tended to be lower in the occluded lung parenchyma than in the patent lung parenchyma but statistical significance was not reached (all, p >0.05). Moreover, significant differences were not found in any ventilation parameters between patent and occluded lung parenchyma in dogs (all, p >0.05). On the other hand, in a swine model of bronchial occlusion, all values of ventilation parameters except K value during the washout period showed significant differences between the occluded lung parenchyma and the patent lung parenchyma. Maximal attenuation, maximal slopes during washin and washout period, and K value at washin were

significantly lower in occluded lung parenchyma than in patent lung parenchyma (all, p <0.05). TTP showed significant delay in occluded segment (p =0.027).

Between-parenchyma absolute differences in maximal enhancement, maximal slope and K value during the washin period, and TTP was greater in pigs than in dogs (all, p <0.05) (Table 3). However, between-parenchyma differences in maximal slope and K value during the washout period was not different between both animals (all, p >0.05). Regarding comparison of between-parenchyma normalized percentage differences between both animals, there were significant differences in all ventilation parameters apart from K value during the washout period (Table 4).

Table 1. CT attenuation according to xenon concentration

Xenon concentration	140 kV image	80 kV image	Mixed image	Xenon map
0%	−1010 HU	−1007 HU	−1008 HU	0 HU
20%	−995 HU	−982 HU	−991 HU	16 HU
60%	−959 HU	−916 HU	−946 HU	55 HU
90%	−926 HU	−859 HU	−907 HU	87 HU

HU= Hounsfield unit

Table 2. Ventilation parameters in both animal models of bronchial occlusion

Canine models of bronchial occlusion (n = 8)			
	Patent lung	Occluded lung	*p* value*
A value (HU)	47.20 ± 6.02	44.41 ± 8.01	0.123
Maximal slope$_{washin}$	6.30 ± 2.84	4.71 ± 1.93	0.068
Maximal slope$_{washout}$	−10.60 ± 2.80	−8.64 ± 2.81	0.092
K_{washin} (sec^{-1})	0.0039 ± 0.0007	0.0038 ± 0.0007	0.892
$K_{washout}$ (sec^{-1})	0.0234 ± 0.0074	0.0208 ± 0	0.317
Time to peak (sec)	142.50 ± 20.72	147.00 ± 27.02	0.892
Swine models of bronchial occlusion (n = 6)			
	Patent lung	Occluded lung	*p* value*
A value (HU)	41.30 ± 5.87	8.32 ± 1.13	0.027
Maximal slope$_{washin}$	5.06 ± 1.47	1.02 ± 0.21	0.027
Maximal slope$_{washout}$	−10.19 ± 1.72	−1.55 ± 1.41	0.028
K_{washin} (sec^{-1})	0.0039 ± 0.0003	0.0026 ± 0.0006	0.027
$K_{washout}$ (sec^{-1})	0.0208 ± 0	0.0139 ± 0.0108	0.157
Time to peak (sec)	140 ± 9.80	212 ± 53.47	0.027

*Wilcoxon matched−pairs signed rank test

Table 3. Comparison of between-parenchyma absolute differences in ventilation parameters between both animal models of bronchial occlusion

	Canine models	Swine models	*p* value*
A value (HU)	−2.79 ± 5.95	−32.97 ± 5.00	0.001
Maximal $slope_{washin}$	−1.59 ± 1.80	−4.63 ± 1.52	0.013
Maximal $slope_{washout}$	1.96 ± 2.81	5.43 ± 4.31	0.228
K_{washin} (sec^{-1})	−0.0001 ± 0.0012	−0.0013 ± 0.0006	0.043
$K_{washout}$ (sec^{-1})	−0.0026 ± 0.0074	0	0.755
Time to peak (sec)	4.50 ± 42.52	72 ± 50.34	0.020

* Mann-Whitney U-test

Table 4. Comparison of between-parenchyma normalized percentage differences in ventilation parameters between both animal models of bronchial occlusion

	Canine models	Swine models	*p* value*
A value	−5.44 ± 16.37	−79.79 ± 1.75	0.0007
Maximal slope$_{washin}$	−20.82 ± 25.28	−80.13 ± 3.92	0.0007
Maximal slope$_{washout}$	16.07 ± 31.03	77.78 ± 8.72	0.004
K_{washin}	−1.43 ± 30.67	−32.77 ± 15.57	0.02
$K_{washout}$	−6.25 ± 17.68	0	0.683
Time to peak	6.75 ± 33.54	51.11 ± 34.43	0.0127

* Mann-Whitney U-test

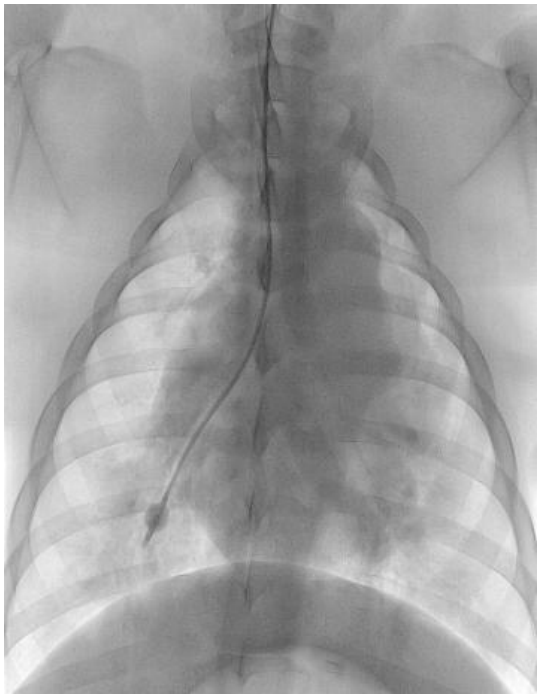

Figure 1. Bronchial occlusion using an occlusion balloon catheter.

Balloon catheter was placed in the posterior segmental bronchus of the right caudal lobe.

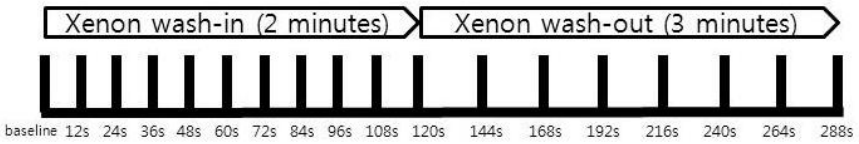

Figure 2. Diagram of Xenon-enhanced dynamic dual energy CT protocol. Total number of scans was 18; one baseline scan, 12 s-interval 10 scans during 2 minute washin period, and 24 s-interval 7 scans during 3 minute washout period.

(A)

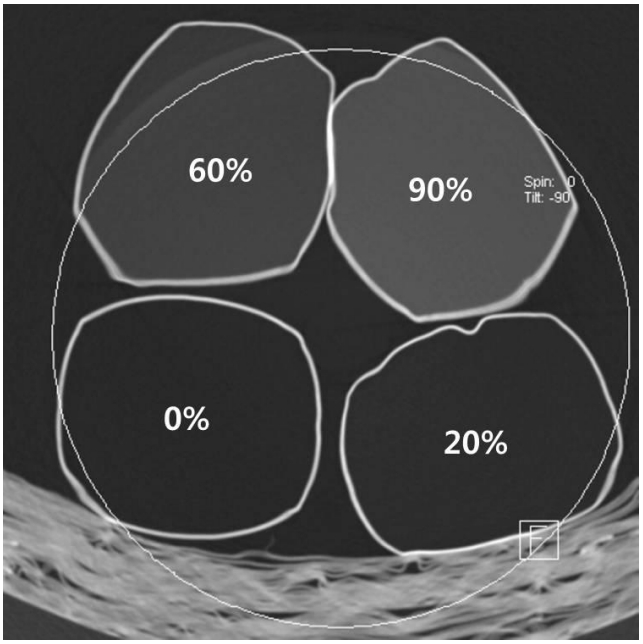

(B)

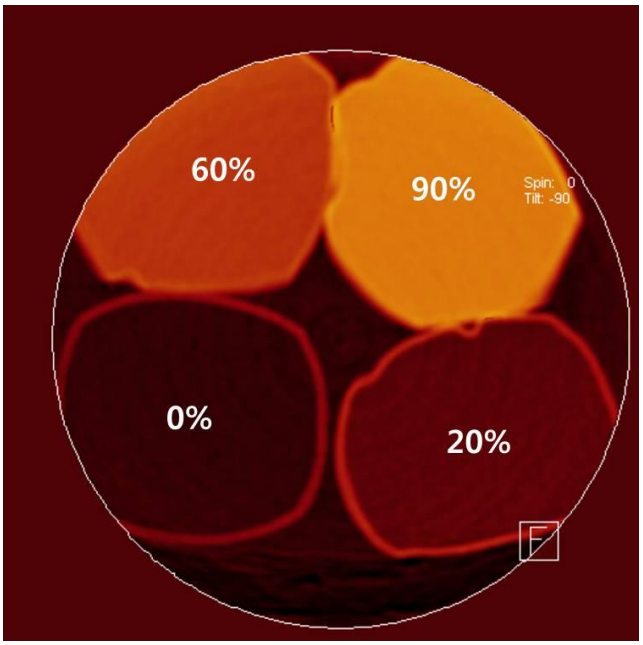

(C)

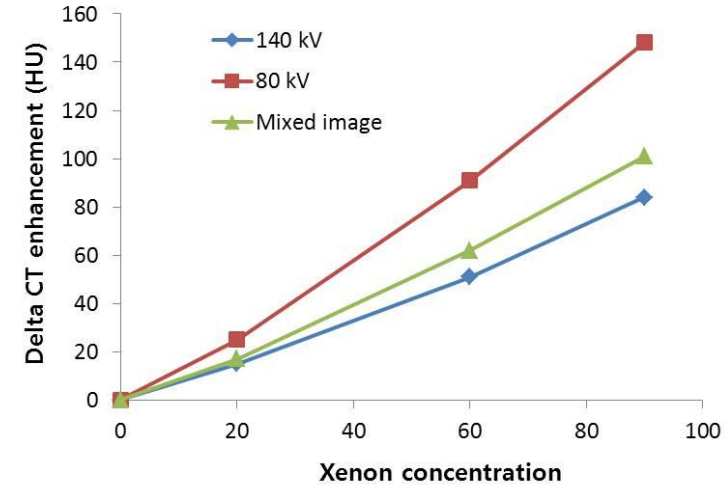

(D)

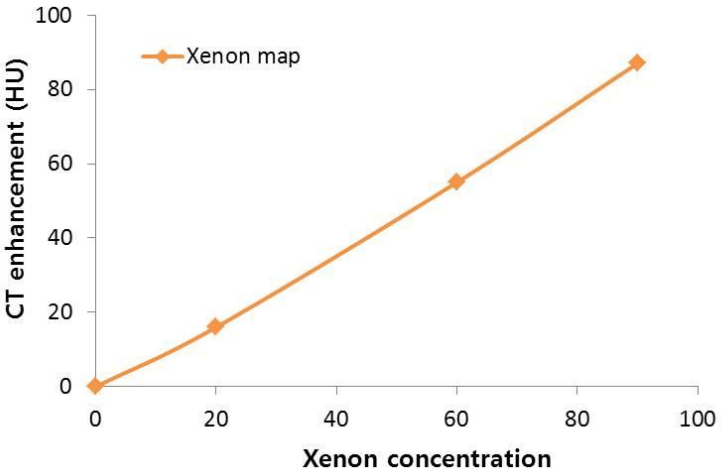

Figure 3. Xenon concentration vs. CT contrast enhancement.

(A) The mixed image close to an approximately 120 kV image. (B) Xenon map. (C) Delta CT enhancement at 80 kV, 140 kV and mixed images according to xenon concentration. (D) CT number at xenon map according to xenon concentration.

(A)

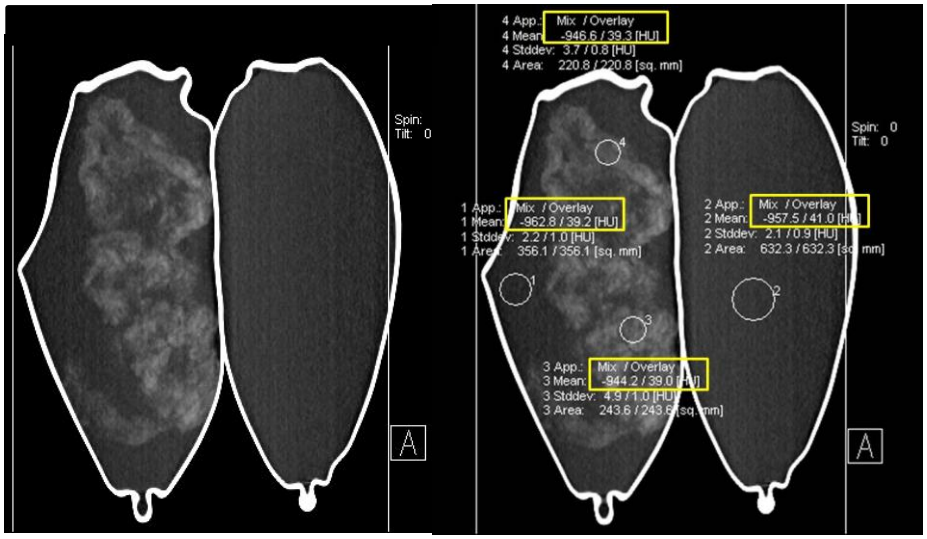

(B)

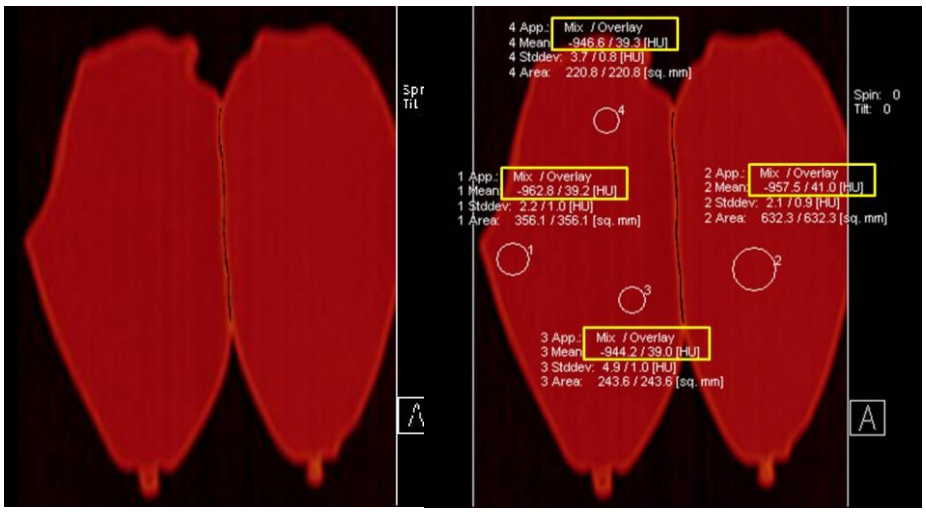

Figure 4. Phantom experiment for the validation of the influence of baseline densities on the attenuation of xenon map. There are two kinds of rubber bags. The left bag contains cottons mimicking lung parenchyma and the right bag is empty. Xenon

with concentrations of 30% was delivered to both bags. Images were taken by dual energy technique of dual source CT.

(A) Mixed image. (B) Xenon map. Mix indicates mixed image. Overlay indicates xenon map. Mean and Stddev indicate mean value and standard deviation of densities measured in the circular region of interest, respectively. Area indicates the area of region of interest. HU indicates Hounsfield units. CT number around artificial cottons is higher up to 20 HU, compared to that of the air. On the other hand, CT number is consistently similar as approximately 40 HU anywhere. It suggests virtual xenon map would be less influenced by variability of basal lung density due to the different respiration level.

(A)

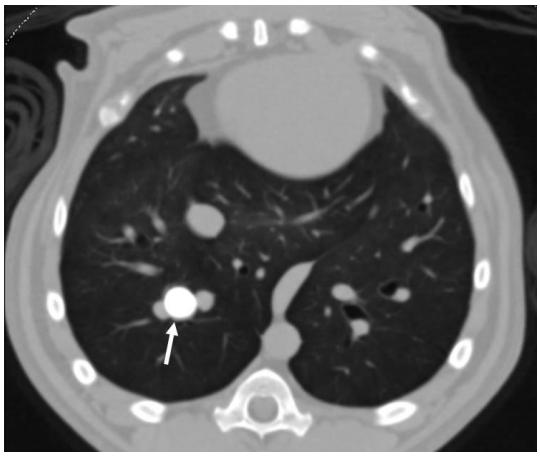

(B)

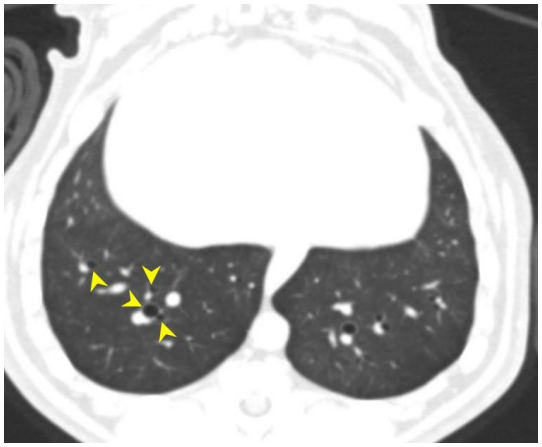

(C)

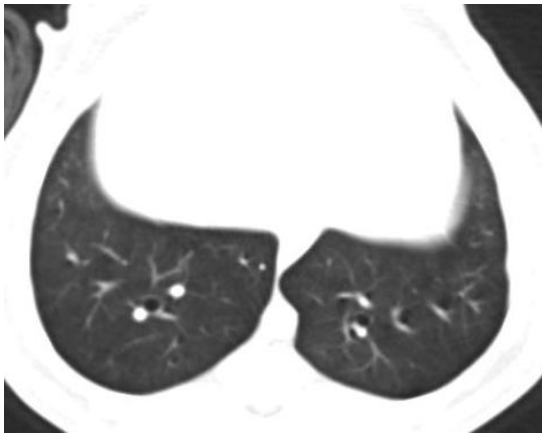

(D)

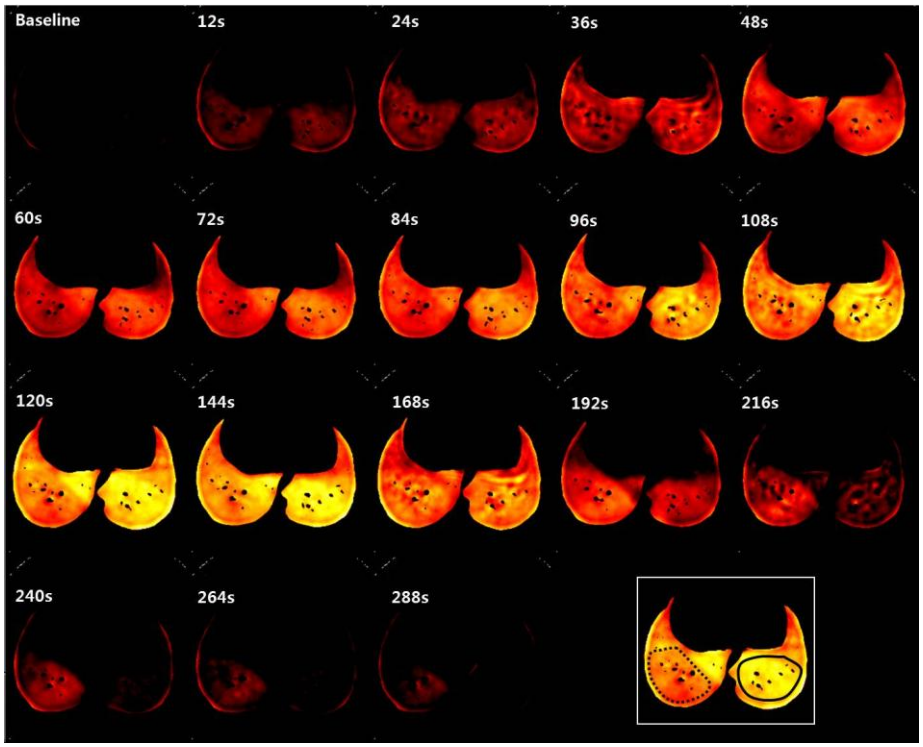
Baseline
12s
24s
36s
48s
60s
72s
84s
96s
108s
120s
144s
168s
192s
216s
240s
264s
288s

(E)

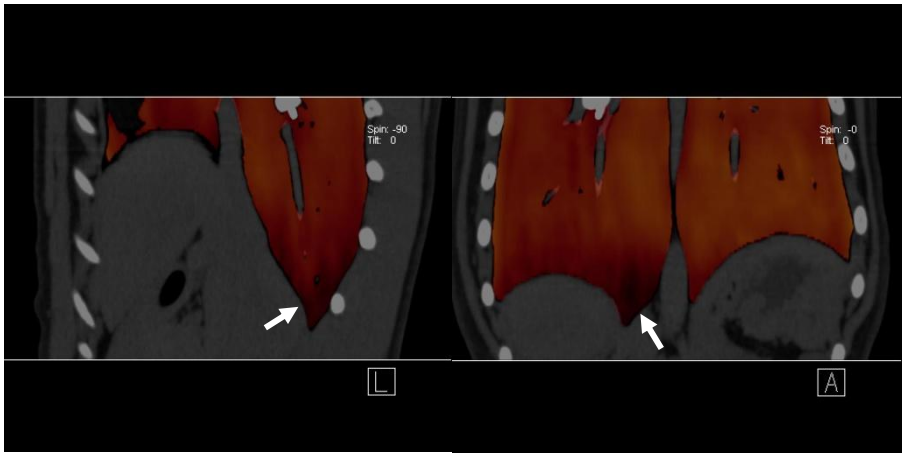
Spin: -90
Tilt: 0
L
Spin: -0
Tilt: 0
A

(F)

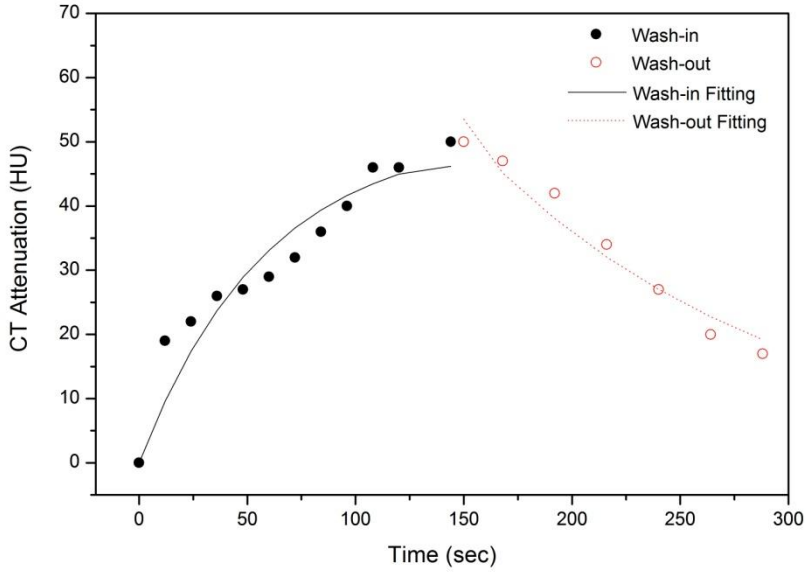
Wash-in
Wash-out
Wash-in Fitting
Wash-out Fitting
CT Attenuation (HU)
Time (sec)
0
10
20
30
40
50
60
70
0
50
100
150
200
250
300

(G)

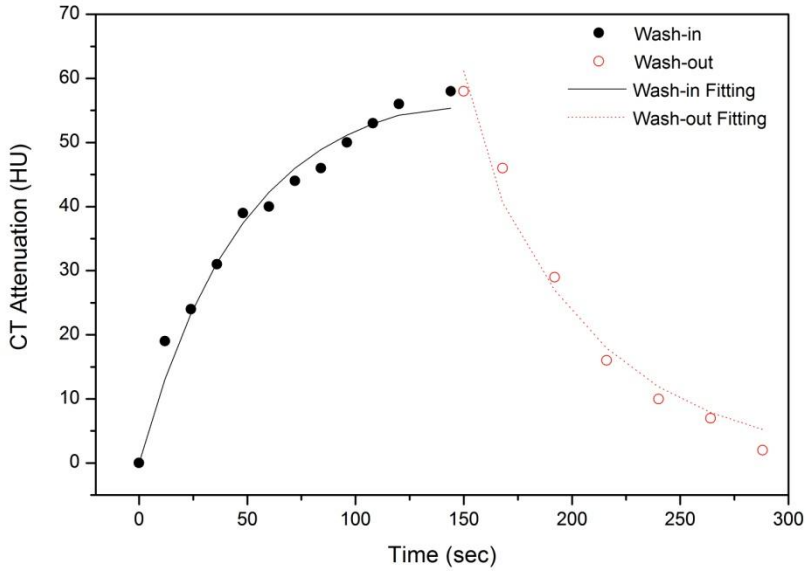
Wash-in
Wash-out
Wash-in Fitting
Wash-out Fitting
CT Attenuation (HU)
Time (sec)
0
10
20
30
40
50
60
70
0
50
100
150
200
250
300

Figure 5. Representative example of xenon ventilation scan in a dog model of bronchial occlusion. (A) Transverse CT image shows a balloon catheter (arrow) placed in the posterior segmental bronchus of the right caudal lobe. (B) Several distal bronchi (arrowheads) were occluded. (C) CT taken 1 hour after balloon inflation demonstrated that atelectasis of occluded segment did not develop. (D) On dynamic scans of xenon map, the occluded lung parenchyma showed minimally decreased xenon enhancement during the washin period, and slight delay of xenon excretion during the washout period, compared to the patent lung parenchyma. Dotted line and solid line indicate regions of interest in the occluded and patent lung parenchyma, respectively. (E) Sagittal (left) and coronal (right) images taken at the end of washin period (120 sec) showed overview of collateral ventilation of the lung parenchyma with airway balloon occlusion. Compared to patent lung, xenon attenuation is slightly decreased. Decrease in xenon enhancement at the lowest portion of the periphery is prominent (arrow). (F) Xenon attenuation curve in occluded the lung parenchyma. (G) Xenon attenuation curve in the patent lung parenchyma.

(A)

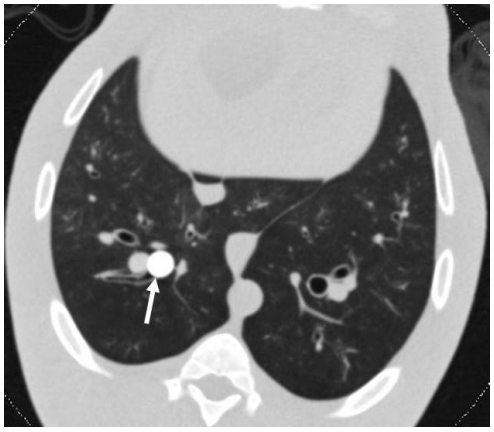

(B)

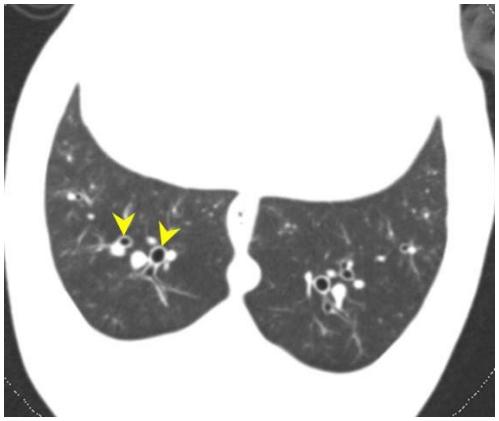

(C)

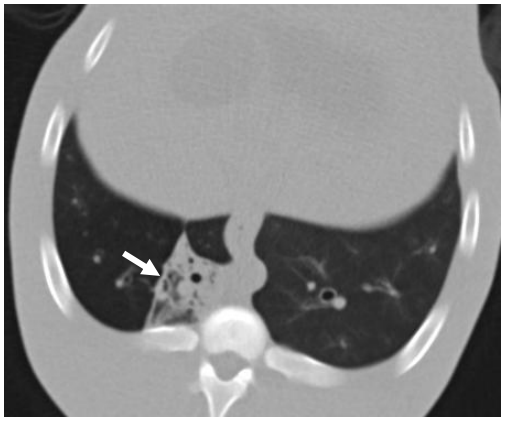

(D)

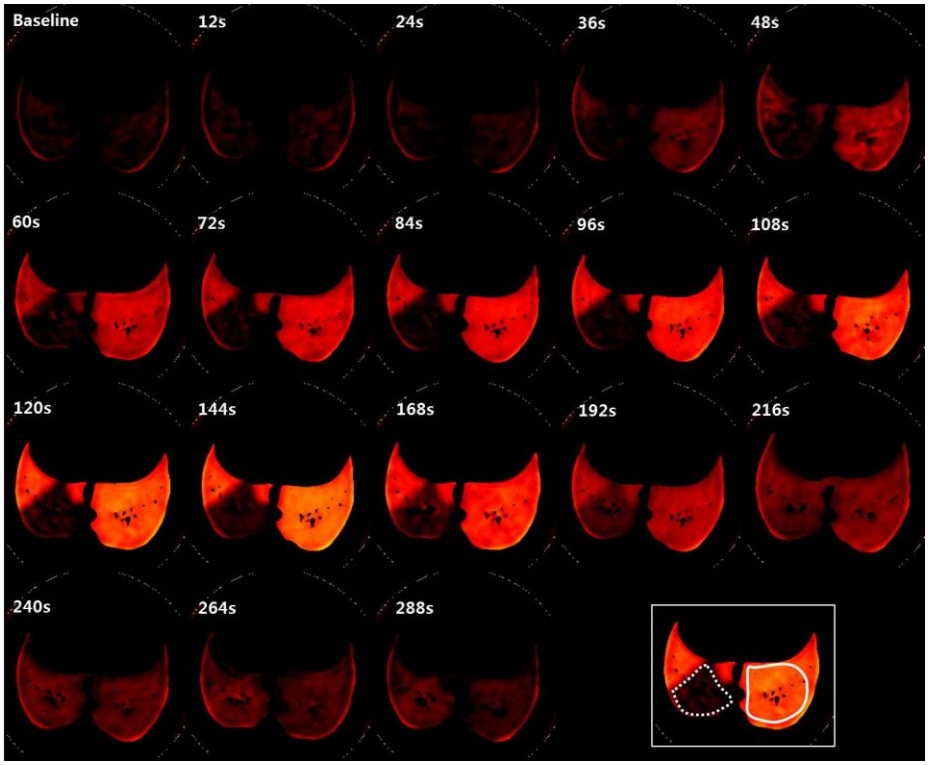
Baseline
12s
24s
36s
48s
60s
72s
84s
96s
108s
120s
144s
168s
192s
216s
240s
264s
288s

(E)

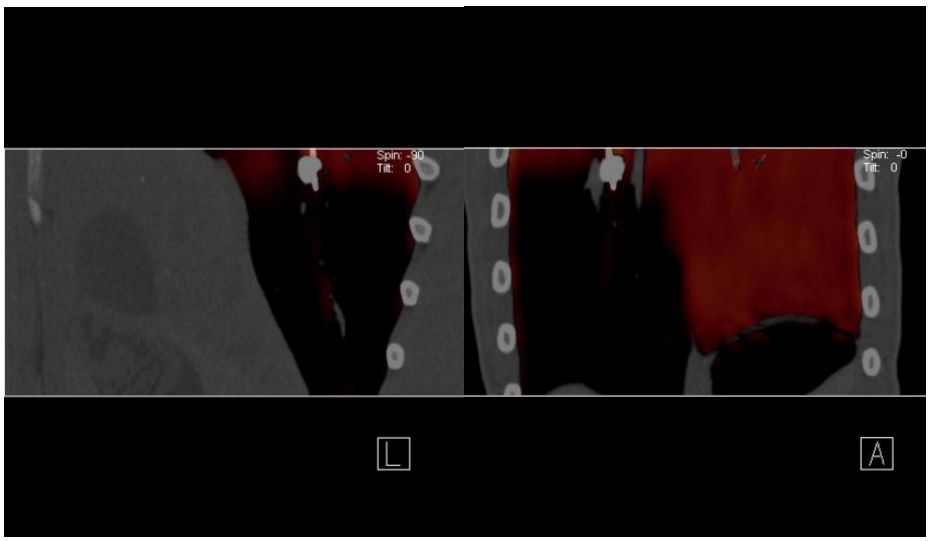
Spin: -90
Tilt: 0
Spin: -0
Tilt: 0
L
A

(F)

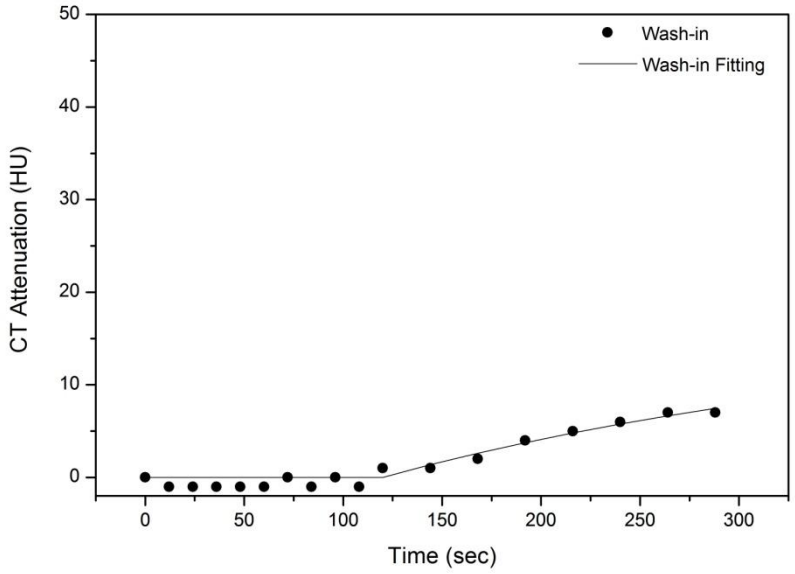
Wash-in
Wash-in Fitting
CT Attenuation (HU)
Time (sec)
0
10
20
30
40
50
0
50
100
150
200
250
300

(G)

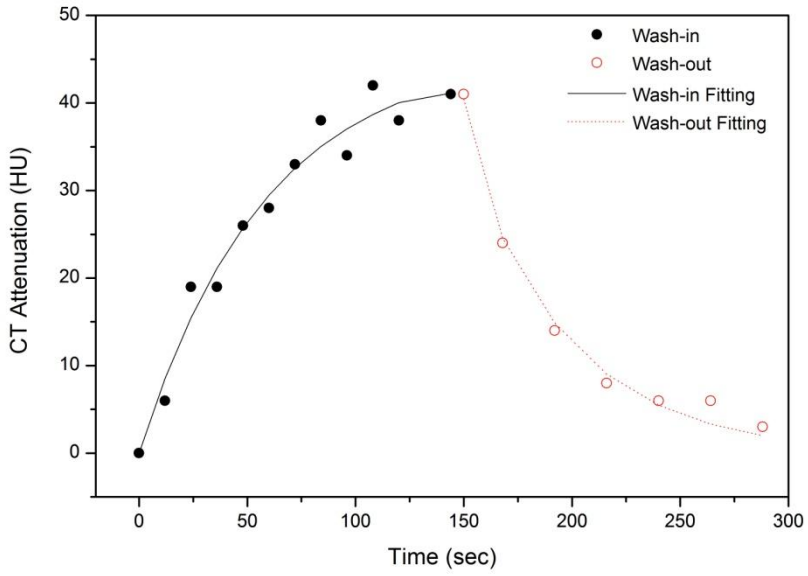
Wash-in
Wash-out
Wash-in Fitting
Wash-out Fitting
CT Attenuation (HU)
Time (sec)
0
10
20
30
40
50
0
50
100
150
200
250
300

Figure 6. Representative example of xenon ventilation scan in a pig model of bronchial occlusion. (A) Transverse CT image shows a balloon catheter (arrow) placed in the posterior segmental bronchus of the right caudal lobe. (B) Several distal bronchi (arrowheads) were occluded. (C) CT taken 1 hour after balloon inflation showed atelectasis (arrow) of occluded segment. (D) On dynamic scans of xenon map, the lung parenchyma with occluded bronchus showed markedly decreased and delayed xenon ventilation during the washin period, and continuous increase in xenon attenuation even during the wash out period, compared to the patent lung parenchyma. Dotted line and solid line indicate regions of interest in the occluded and patent lung parenchyma, respectively. (E) Sagittal (left) and coronal (right) images showed taken at the end of washin period (120 sec) overview of collateral ventilation of the lung parenchyma with airway balloon occlusion. Compared to patent lung, xenon attenuation is markedly decreased. (F) Xenon attenuation curve in the occluded lung parenchyma. (G) Xenon attenuation curve in the patent lung parenchyma.

DISCUSSION

This study demonstrated that significant difference in collateral ventilation between different species of animals could be quantified using xenon-enhanced dynamic dual energy CT. Xenon-enhanced dynamic dual energy CT can be used for predicting prognosis after bronchoscopic lung volume reduction in patients with emphysema by quantitatively assessing collateral ventilation which hinders the successful collapse of nonfunctioning lung after procedure. Furthermore, it can be also used for evaluating functional status of other diseased lung by using quantitative ventilation parameters based on Kety model.

Collateral channels in the normal human lung are well described previously: 1-2 μm interalveolar pores of Kohn (3), 30 μm bronchioloalveolar channels of Lambert (43) and 80-150 μm interbronchiolar channels of Martin (6). The resistance of the collateral channels in normal human lungs was found to be 260-3300 cm H_2O/l/s (7,44,45), or approximately 100-500 times the resistance of the regular branching airways. However, in emphysema, whereas airway resistance is typically increased, collateral resistance may be as low as 5-16 cm H_2O/l/s (1,7,44,46), less than the resistance of the regular

branching airways. Therefore, in emphysema airflow to some regions may occur preferentially via collateral channels rather than through the narrowed airways (1). In addition, interlobar collateral flow can even occur in emphysema (7,47). In fact, collateral ventilation has a positive role in gas exchange in patients with various disease entities including emphysema, bronchiolitis obliterans, bronchiectasis or bronchial atresia. However, its role has changed negatively with the emergence of new bronchoscopic techniques for treating emphysema, and have been explained as the cause of failure of EBVs to produce segmental or lobar atelectasis in most patients (2).

Collateral ventilation has been previously assessed using several different methods: postmortem ex vivo experiments (3,6-8,43-45,47-51), and in vivo studies using bronchoscopic measurement (1,26,40,46), ^{133}Xe (52,53), conventional CT (54-56) and xenon ventilation CT (38). Most studies were limited to ex vivo experiments. A simple and accurate in vivo technique to measure collateral ventilation is needed for evaluating its therapeutic implication. In vivo bronchoscopic measurement involves placing the bronchoscope in wedge position and introducing a constant flow of gas

through the working channel until a steady-state pressure reached. When the flow of gas is interrupted, the drop in pressure can be used to directly calculate the resistance to collateral flow (1,44). The subsequent exponential decline in pressure can be used to calculate the time constant for collateral ventilation and the compliance of the occluded segment (1,44). They found an initial abrupt fall and subsequent slow decay of intrasegmental pressure in emphysema in human and sheep model, compared to continuous fall in pressure in normal lung (1,44).

Conventional CT can also assess collateral ventilation indirectly. Higuchi et al. (55) found complete fissure and heterogeneity of emphysema on CT were associated with absence of interlobar collaterals. However, completeness of fissure showed very low accuracy of 52% for predicting no collateral ventilation with positive and negative predictive values of 63% and 29%, respectively. Heterogeneity CT score of emphysema also showed modest accuracy of 75% with positive and negative predictive values of 90% and 60%, respectively. Furthermore, this evaluation is limited to binary one, presence or absence of collateral ventilation at the

interlobar level, instead of quantifying the amount of collateral flow even though the amount of collateral ventilation is likely to be a continuous variable.

Recently, Herth et al. (26) evaluated the efficacy of Chartis pulmonary assessment of collateral ventilation for predicting outcome of EBVs therapy to significant target lobe volume reduction. After a balloon catheter is inserted via the working channel of the bronchoscope, balloon inflation occludes the airway, blocking the flow of inspired air and allowing air to flow out only through the central lumen of the catheter. Chartis pulmonary assessment system reads the pattern of the flow and pressure in real time on a console: gradually reduced air flow out pattern indicating no collateral ventilation versus a continuous flow indicating the presence of collateral ventilation. They reported an overall accuracy of 75% with positive and negative predictive values of 83% and 71%, respectively. They explained collapse of the bronchial wall distal to the inflated balloon or large collateral channels causing a reverse flow to adjacent lobe for the false negative assessment. Even in the presence of collateral channels, 17% of collateral ventilation positive patients showed effective volume reduction. They

assumed that it could be attributed to relatively small caliber with high resistance. It suggests that prediction of collateral ventilation is still challenging. Xenon ventilation CT can play a complementary role for measuring collateral ventilation (38,39). The present study suggests the possibility of quantifying ventilation parameters according to different degree of collateral channels. In dog models representing good development of collateral channel, there were no significant differences in ventilation parameters. These results are in general accord with those of a previous study by Chae et al (38). The minor different point is that A and K values during washin of occluded segment tended to be much smaller than those of patent segment although insignificant. Location and size of ROIs can be the cause for the difference. Whereas big ROIs as replacing the occluded segment were applied in our study, smaller ROIs were applied in their study. Therefore, smaller ROIs might have chances to be located in central portions decreasing xenon ventilation. In pig models representing poor development of collateral channel, we found obviously significant differences in ventilation parameters between patent and occluded lungs. Interestingly, we observed

continuous increase in CT attenuation during washout period even though enhancement was minimal and its starting point was much delayed. Although minimal, collateral channels could be attributed to this phenomenon. Several investigators also observed continuous increase in CT attenuation during washout phase in diseased human lung parenchyma including emphysema, bronchial atresia, or air trapping (36,37,39).

Our study has several limitations. First, Kety model assumes xenon as insoluble but, in fact, xenon is moderately soluble in the blood (solubility coefficient = 0.115). Therefore, there have a chance that recirculated xenon in returning blood flow would influence on lung attenuation measured during washin and washout periods. The previous study by Hoag et al. (57) , in which they blocked either side of a mainstream bronchus and performed CT 1 min and 5 min after ventilation with 60% xenon in mongrel canines, found that there was no change in attenuation, even over the 5 min after xenon ventilation. Therefore, we believe that xenon enhancement of occluded segment was mainly caused by collateral ventilation. Second, there can be an argument that bronchial obstruction was complete. Assuming from the fact that bronchial occlusion

was performed in an identical method in both animals and occluded lung segment collapsed 1 hour after bronchial occlusion in all pigs, we believe that complete bronchial occlusion was effectively performed in both animals. Third, we were unable to measure washout ventilation parameters in two pigs because of continuous increase in xenon attenuation even in washout period presumably via small collateral ventilation and therefore, the relatively short data of washout period. Therefore, our animal numbers were too small for an adequate statistical work-up. Fourth, xenon map generated by three decomposition theory is a virtual image. The accuracy of xenon map was not validated yet. However, based on our phantom study, we believe that effect of underlying tissue lung density on xenon attenuation on xenon enhanced images would be minor, even although current dual energy technique is not perfect. Fifth, high radiation exposure due to repetitive temporal scans can be problematic in clinical application. Although repetitive temporal scans are necessary for quantifying ventilation parameters, we found the most significant difference in maximal enhancement between two animal models. This suggests single phase of washin period

could predict the degree of collateral ventilation using measuring simple xenon attenuation in the lung. However, further validation study for this may be needed. Sixth, degree of collateral channels between dogs and pigs was not proven pathologically in our study. However, collateral resistance and time constant in these animals have been previously well established: 0.13−1.75 cm H_2O/l/s for collateral resistance and 0.13−0.40 sec for time constant of dogs, and too high to measure for collateral resistance and 92−234 sec for time constant of pigs (1,2,40). Lastly, we selected canine and swine model of bronchial obstruction representing extreme cases for development of collateral channels. Further studies using swine model with emphysema might be needed in order to validate efficacy of xenon ventilation CT for detecting various degree of collateral ventilation.

In conclusion, xenon−enhanced, dynamic dual energy technique of dual source CT allows quantifying collateral ventilation and detecting its difference between canine and swine models of bronchial obstruction.

REFERENCES

1. Tsai LW, Hoffman AM, Mazan MR, Ingenito EP. Bronchoscopic measurement of collateral ventilation in a sheep model of emphysema. Respiration 2007;74:565-571.
2. Cetti EJ, Moore AJ, Geddes DM. Collateral ventilation. Thorax 2006;61:371-373.
3. Kohn HN. Zur Histologie der indurirenden fibrinosen Pneumonie. Munch Med Wochenschr 1893;40:42-45.
4. Van Allen CM, Lindskog GE, Richter HG. Gaseous Interchange Between Adjacent Lung Lobules. Yale J Biol Med 1930;2:297-300.
5. McLaughlin RF, Tyler WS, Canada RO. A study of the subgross pulmonary anatomy in various mammals. Am J Anat 1961;108:149-165.
6. Martin HB. Respiratory bronchioles as the pathway for collateral ventilation. J Appl Phsyiol 1966;21:1443-1447.
7. Hogg JC, Macklem PT, Thurlbeck WM. The resistance of collateral channels in excised human lungs. J Clin Invest 1969;48:421-431.

8. Macklem PT. Airway obstruction and collateral ventilation. Physiol Rev 1971;51:368-436.

9. MacNee W. Update in chronic obstructive pulmonary disease 2007. Am J Respir Crit Care Med 2008;177:820-829.

10. GOLD (2010) Global strategy for the diagnosis, management, and prevention of chronic obstructive pulmonary disease. Executive summery, updated:http://www.goldcopd.org.

11. Han MK, Agusti A, Calverley PM, et al. Chronic obstructive pulmonary disease phenotypes: the future of COPD. Am J Respir Crit Care Med 2010;182:598-604.

12. Miravitlles M, Calle M, Soler-Cataluna JJ. Clinical phenotypes of COPD: identification, definition and implications for guidelines. Arch Bronconeumol 2012;48:86-98.

13. Taneja A. Bronchoscopic interventions in the management of chronic obstructive pulmonary disease. Curr Opin Pulm Med 2013;19:145-151.

14. Criner GJ, Sternberg AL. National Emphysema Treatment Trial: the major outcomes of lung volume

reduction surgery in severe emphysema. Proc Am Thorac Soc 2008;5:393-405.

15. Fishman A, Martinez F, Naunheim K, et al. A randomized trial comparing lung-volume-reduction surgery with medical therapy for severe emphysema. N Engl J Med 2003;348:2059-2073.

16. Leggett RJ, Flenley DC. Portable oxygen and exercise tolerance in patients with chronic hypoxic cor pulmonale. Br Med J 1977;2:84-86.

17. Ries AL, Make BJ, Reilly JJ. Pulmonary rehabilitation in emphysema. Proc Am Thorac Soc 2008;5:524-529.

18. Snell GI, Holsworth L, Borrill ZL, et al. The potential for bronchoscopic lung volume reduction using bronchial prostheses: a pilot study. Chest 2003;124:1073-1080.

19. Wan IY, Toma TP, Geddes DM, et al. Bronchoscopic lung volume reduction for end-stage emphysema: report on the first 98 patients. Chest 2006;129:518-526.

20. Strange C, Herth FJ, Kovitz KL, et al. Design of the Endobronchial Valve for Emphysema Palliation Trial (VENT): a non-surgical method of lung volume reduction. BMC Pulm Med 2007;7:10.

21. Slebos DJ, Klooster K, Ernst A, Herth FJ, Kerstjens HA. Bronchoscopic lung volume reduction coil treatment of patients with severe heterogeneous emphysema. Chest 2012;142:574-582.

22. Gompelmann D, Heussel CP, Eberhardt R, et al. Efficacy of bronchoscopic thermal vapor ablation and lobar fissure completeness in patients with heterogeneous emphysema. Respiration 2012;83:400-406.

23. Herth FJ, Gompelmann D, Stanzel F, et al. Treatment of advanced emphysema with emphysematous lung sealant (AeriSeal(R)). Respiration 2011;82:36-45.

24. Kramer MR, Refaely Y, Maimon N, Rosengarten D, Fruchter O. Bilateral endoscopic sealant lung volume reduction therapy for advanced emphysema. Chest 2012;142:1111-1117.

25. Magnussen H, Kramer MR, Kirsten AM, et al. Effect of fissure integrity on lung volume reduction using a polymer sealant in advanced emphysema. Thorax 2012;67:302-308.

26. Herth FJ, Eberhardt R, Gompelmann D, et al. Radiological and clinical outcomes of using Chartis to plan

endobronchial valve treatment. Eur Respir J 2013;41:302-308.

27. Sciurba FC, Ernst A, Herth FJ, et al. A randomized study of endobronchial valves for advanced emphysema. N Engl J Med 2010;363:1233-1244.

28. Gur D, Drayer BP, Borovetz HS, Griffith BP, Hardesty RL, Wolfson SK. Dynamic computed tomography of the lung: regional ventilation measurements. J Comput Assist Tomogr 1979;3:749-753.

29. Gur D, Shabason L, Borovetz HS, et al. Regional pulmonary ventilation measurements by xenon enhanced dynamic computed tomography: an update. J Comput Assist Tomogr 1981;5:678-683.

30. Snyder JV, Pennock B, Herbert D, et al. Local lung ventilation in critically ill patients using nonradioactive xenon-enhanced transmission computed tomography. Crit Care Med 1984;12:46-51.

31. Winkler SS, Nielsen A, Mesina J. Respiratory depression in goats by stable xenon: implications for CT studies. J Comput Assist Tomogr 1987;11:496-498.

32. Murphy DM, Nicewicz JT, Zabbatino SM, Moore RA. Local pulmonary ventilation using nonradioactive xenon-enhanced ultrafast computed tomography. Chest 1989;96:799-804.

33. Marcucci C, Nyhan D, Simon BA. Distribution of pulmonary ventilation using Xe-enhanced computed tomography in prone and supine dogs. J Appl Physiol 2001;90:421-430.

34. Tajik JK, Chon D, Won C, Tran BQ, Hoffman EA. Subsecond multisection CT of regional pulmonary ventilation. Acad Radiol 2002;9:130-146.

35. Chon D, Simon BA, Beck KC, et al. Differences in regional wash-in and wash-out time constants for xenon-CT ventilation studies. Respir Physiol Neurobiol 2005;148:65-83.

36. Chae EJ, Seo JB, Goo HW, et al. Xenon ventilation CT with a dual-energy technique of dual-source CT: initial experience. Radiology 2008;248:615-624.

37. Goo HW, Chae EJ, Seo JB, Hong SJ. Xenon ventilation CT using a dual-source dual-energy technique: dynamic

ventilation abnormality in a child with bronchial atresia. Pediatr Radiol 2008;38:1113-1116.

38. Chae EJ, Seo JB, Kim N, et al. Collateral ventilation in a canine model with bronchial obstruction: assessment with xenon-enhanced dual-energy CT. Radiology 2010;255:790-798.

39. Park EA, Goo JM, Park SJ, et al. Chronic obstructive pulmonary disease: quantitative and visual ventilation pattern analysis at xenon ventilation CT performed by using a dual-energy technique. Radiology 2010;256:985-997.

40. Robinson NE, Sorenson PR. Collateral flow resistance and time constants in dog and horse lungs. J Appl Physiol 1978;44:63-68.

41. Delaunois L. Anatomy and physiology of collateral respiratory pathways. Eur Respir J 1989;2:893-904.

42. Kety SS. The theory and applications of the exchange of inert gas at the lungs and tissues. Pharmacol Rev 1951;3:1-41.

43. Lambert MW. Accessory bronchiole-alveolar communications. J Pathol Bacteriol 1955;70:311-314.

44. Terry PB, Traystman RJ, Newball HH, Batra G, Menkes HA. Collateral ventilation in man. N Engl J Med 1978;298:10-15.

45. Berend N, Skoog C, Thurlbeck WM. Collateral ventilation in excised human lungs. J Appl Physiol 1981;50:927-930.

46. Morrell NW, Wignall BK, Biggs T, Seed WA. Collateral ventilation and gas exchange in emphysema. Am J Respir Crit Care Med 1994;150:635-641.

47. Rosenberg DE, Lyons HA. Collateral ventilation in excised human lungs. Respiration 1979;37:125-134.

48. Baarsma PR, Dirken MN. Collateral ventilation. J Thorac Surg 1948;17:238-251.

49. Baarsma PR, Dirken MN, Huizinga E. Collateral ventilation in man. J Thorac Surg 1948;17:252-263.

50. Menkes HA, Traystman RJ. Collateral ventilation. Am Rev Respir Dis 1977;116:287-309.

51. Kuriyama T, Wagner WW, Jr. Collateral ventilation may protect against high-altitude pulmonary hypertension. J Appl Physiol 1981;51:1251-1256.

52. Effmann EL, Freedman GS, Lange RC. 133Xe studies of collateral ventilation and air trapping following endobronchial occlusion. Radiology 1972;105:85-91.

53. Salanitri J, Kalff V, Kelly M, Holsworth L, Williams T, Snell G. 133Xenon ventilation scintigraphy applied to bronchoscopic lung volume reduction techniques for emphysema: relevance of interlobar collaterals. Intern Med J 2005;35:97-103.

54. Nakano Y, Coxson HO, Bosan S, et al. Core to rind distribution of severe emphysema predicts outcome of lung volume reduction surgery. Am J Respir Crit Care Med 2001;164:2195-2199.

55. Higuchi T, Reed A, Oto T, et al. Relation of interlobar collaterals to radiological heterogeneity in severe emphysema. Thorax 2006;61:409-413.

56. Washko GR, Martinez FJ, Hoffman EA, et al. Physiological and computed tomographic predictors of outcome from lung volume reduction surgery. Am J Respir Crit Care Med 2010;181:494-500.

57. Hoag JB, Fuld M, Brown RH, Simon BA. Recirculation of inhaled xenon does not alter lung CT density. Acad Radiol 2007;14:81-84.

국문 초록

서론: 본 연구의 목적은 이중선원의 이중에너지 기법을 이용한 제논 조영증강 동적 영상을 통해 산출된 정량적 환기변수들이 기관지를 폐색한 개와 돼지 모델에서의 측부환기량의 차이를 발견할 수 있는지를 알아보고자 하였다. 이를 통해 측부환기량 정량화에 대한 제논 조영증강 영상의 유용성을 평가하고자 하였다.

방법: 25-30 kg 의 여덟 마리 개와 여섯 마리 돼지를 이용하여 전신마취 하에 실험하였다. 투시 유도 하에 11.5 mm 의 표준 폐색 풍선 카테터를 이용하여 미엽의 후분절기관지를 폐색하였다. 이중선원의 이중에너지 기법(51 eff. mAs/213 eff. mAs at 140 kV/80 kV)을 이용하여 한번의 기저스캔 후 2 분 wahsin 기간 (인공호흡기를 통하여 60% 제논 흡입)동안 12 초 간격으로 12 번의 스캔, 3 분 washout 기간동안 24 초 간격으로 7 번의 CT 를 시행하였다. 전용 소프트웨어를 통하여 120 kV 에 해당하는 혼합영상과 제논 영상을 얻은 후, 동적 제논 영상의 시간 밀도 곡선을 Kety 모델에 입각하여 최대 제논 밀도 (A 수치), 최대 기울기, 환기속도 (K 수치), 최고밀도에 도달하는 시간 등 정량적 환기 변수들을 산출하였다.

결과: 개와 돼지 모델 모두에서 폐색된 폐분절 부위의 최대 제논 밀도가 낮았으나 돼지모델에서만 유의성을 보였다 (개모델, 44.4 ± 8.0 HU 대 47.2 ± 6.0 HU, p =0.123; 돼지모델, 8.32 ± 1.1 HU

대 41.3 ± 5.9 HU, p =0.027). 또한 개모델과 비교하였을 때 돼지에서 폐색한 폐분절과 기관지가 개통된 폐분절간의 의미 있게 큰 최대 제논 밀도의 차이를 보였다 (절대 차이 −33.0 ± 5.0 대 −2.8 ± 7.1 HU, p =0.011; 표준화된 백분율 차이 −79.8 ± 1.8% 대 −5.4 ± 16.4%, p =0.0007). 두 모델에서 모두 폐색된 폐분절에서 최대 기울기 수치가 떨어져 있었으나 돼지모델에서만 유의성을 보였다 (p =0.027), 이러한 현상은 washin 와 washout 기간에서 모두 같은 소견을 보였다. 폐색된 부위와 개통된 부위간의 차이도 역시 돼지모델에서 더 큰 차이를 보였다 (p <0.05). 개모델에서의 K 수치의 경우에는 washin 과 washout 기간 모두에서 폐색된 부위와 개통된 부위간의 의미 있는 차이가 없었던 반면 (p >0.05), 돼지모델에서는 washin 기간에서만 K 수치가 의미있는 차이를 보였다 (p <0.05). 한편, 최대 밀도에 도달하는 시간은 개에서는 폐분절간의 의미 있는 차이를 보이지 않는 반면 (p >0.05), 돼지모델에서는 폐색된 폐분절에서 의미 있게 지연되어 있었다 (212 ± 53.5 초 대 140 ± 9.8 초, p =0.027; 표준화된 백분율 차이 51.1 ± 34.4% 대 6.8 ± 33.5%, p =0.013).

결론: 결론적으로 이중선원의 이중에너지 기법을 이용한 제논 조영증강 동적 영상을 통해서 기관지를 폐색한 개와 돼지간의 측부환기량을 차이를 정량화 할 수 있었다. 따라서 제논 환기 CT 를 이용하

여 측부환기량을 정량화함으로써 폐기종환자에서 기관지밸브 삽입 후 의미 있는 폐용적 감소를 예측할 수 있을 것으로 기대된다.

주요어: 만성 폐쇄성 폐 질환, 폐기종, 측부환기, 제논, 이중에너지 CT

학 번: 2007-30957